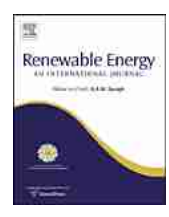


Contents lists available at SciVerse ScienceDirect

Renewable Energy

journal homepage: www.elsevier.com/locate/renene



Numerical sensitivity study of thermal response tests

Valentin Wagner ^{a,*}, Peter Bayer ^b, Markus Kübert ^c, Philipp Blum ^a

- ^a Karlsruhe Institute of Technology (KIT), Institute for Applied Geosciences (AGW), Kaiserstraße 12, 76131 Karlsruhe, Germany
- ^b ETH Zurich, Engineering Geology, Sonneggstrasse 5, 8092 Zürich, Switzerland
- ^c Tewag Technologie Erdwärmeanlagen Umweltschutz GmbH, Am Haag 12, 72181 Starzach-Felldorf, Germany

ARTICLE INFO

Article history: Received 7 March 2011 Accepted 1 November 2011 Available online 3 December 2011

Keywords:
Geothermal energy
Thermal response test
Thermal conductivity
Geothermal gradient
Thermal dispersivity

ABSTRACT

Thermal conductivity and thermal borehole resistance are basic parameters for the technical and sustainable design of closed ground source heat pump (GSHP) systems. One of the most common methods to determine these parameters is the thermal response test (TRT). The response data measured are typically evaluated by the Kelvin line source equation which does not consider all relevant processes of heat transfer in the subsurface. The approach only considers conductive heat transfer from the borehole heat exchanger (BHE) and all transport effects are combined in the parameters of effective thermal conductivity and thermal borehole resistance. In order to examine primary effects in more detail, a sensitivity study based on numerically generated TRT data sets is performed considering the effects of (1) the in-situ position of the U-shaped pipes of borehole heat exchangers (shank spacing), (2) a non-uniform initial thermal distribution (such as a geothermal gradient), and (3) thermal dispersivity. It will be demonstrated that the shank spacing and the non-uniform initial thermal distribution have minor effects (less than 10%) on the effective thermal conductivity and the determined borehole resistance. Constant groundwater velocity with varying thermal dispersivity values, however, has a significant influence on the thermal borehole resistance. These effects are even more pronounced for interpreted effective thermal conductivity which is overestimated by a factor of 1.2–2.9 compared to the real thermal conductivity of the saturated porous media.

© 2011 Elsevier Ltd. All rights reserved.

1. Introduction

The utilization of shallow geothermal energy is becoming increasingly popular, which is mainly due to the rising costs of fossil fuels and its potential to avoid additional or even reduce CO₂ emissions [1,2]. The most popular way to exploit shallow geothermal energy resources is the use of ground source heat pump (GSHP) systems. They extract energy from the ground to depths of about 400 m by horizontal or vertical borehole heat exchangers (BHEs). In the latter, a heat carrier fluid is circulated in closed pipes that transfer heat or cold to the heat pumps. The pipes are installed in boreholes and are often backfilled with a bentonite-cement suspension for safety and stability reasons. To ensure the efficiency of such systems, appropriate dimensioning of the GSHP system is essential. Only if the extracted amount of energy is equal or close to the amount of energy which can be replenished naturally, will the GSHP system work efficiently and sustainably over its lifetime. The extractable amount of energy mainly depends on the thermal properties and the hydrogeological conditions of the ground as well as on the properties of the grouting material.

Thermal properties commonly are estimated in-situ by a thermal response test (TRT) which was developed by Morgensen [3]. During the TRT, a constant amount of energy is injected into [4] or extracted [5] from the ground by using a BHE and the temperature development of the circulating heat carrier fluid is recorded. Standard interpretation of TRTs follows the line source theory [5]. The parameters obtained are the effective thermal conductivity, λ_{eff} , which integrates all thermal effects of the subsurface along the entire BHE length, and the thermal borehole resistance, Rb, which describes the heat transfer inside the entire BHE. To characterize the expected performance of a BHE, all relevant heat transfer processes in the subsurface are parameterized by two integrative terms, $\lambda_{\rm eff}$ and $R_{\rm b}$. However, it is often impossible to identify the reasons of specific parameter values, since the interference of the dominant heat transfer processes cannot be resolved. In order to clarify the role of different effects on $\lambda_{\rm eff}$ and $R_{\rm b}$, several field [6–12] and modelling studies [12–18] were performed. From field studies, it is known that groundwater flow results in an increase of λ_{eff} [6,7]. Esen and Inalli [8] suggested that increasing the depth of the analyzed BHEs yields a decrease of R_b. Variable daily air

^{*} Corresponding author. Tel.: +49 721 608 45065; fax: +49 721 606 279. E-mail address: valentin.wagner@kit.edu (V. Wagner).

Nomenclature		Greek symbols			
		λ	thermal conductivity (W m^{-1} K^{-1})		
T	temperature (°C)	κ	thermal diffusivity ($m^2 s^{-1}$)		
q	heat transfer rate per unit length (W m^{-1})	γ	Euler's constant		
R_b	thermal borehole resistance (m K W^{-1})				
r	radius (m)	Subscri	Subscripts		
t	time (s)	f	fluid		
Ei	exponential integral	bw	borehole wall		
и	integration variable	sub	subsurface		
m	slope of the linear regression (°C)	eff	effective property value		
n	number of time steps evaluated	num	numerically determined		
L	length of the borehole heat exchanger (m)	lin	determined by linear regression		
ср	volumetric heat capacity of the porous media	par	determined by parameter estimation		
•	$(MJ m^{-3}K^{-1})$	m	property of the porous media		
cp_f	volumetric heat capacity of the heat carrier fluid	0	initial or undisturbed value		
- 3	$(MJ m^{-3}K^{-1})$	mea	measured value		
Q_f	volume flow rate of the heat carrier fluid (m ³ s ⁻¹)	in	inflow		
7	,	out	outflow		

temperature causes fluctuations in the recorded temperature time curve of the circulating heat carrier fluid, which introduce uncertainty in TRT interpretation [9]. An enhanced thermal conductivity of the grouting material improves R_b [10]. Increasing heat injection rates of groundwater-filled boreholes results in a decrease of R_b [11]. Raymond et al. [12] demonstrated that geological heterogeneity (e.g. layering) can result in an overestimation of $\lambda_{\rm eff}$. The results of TRT simulations confirm these observations like the enhancing effect on $\lambda_{\rm eff}$ of groundwater flow [13] and reveal the influence of additional parameters, especially of the type of aquifer [14], heat capacity of the subsurface [15], horizontal configuration of the BHE pipes [16], and changes in the heat carrier fluid density during a TRT [17].

The effects of different methods to calculate the mean heat carrier fluid temperature [18] and the impact of vertical temperature variations [12] are analyzed based on numerical models. For example, high values of groundwater flow velocity yield elevated $\lambda_{\rm eff}$ values. Another crucial factor is the shank space defined by Lamarche et al. [19] as the distance between the centres of the BHE pipes. A small shank spacing or a lower thermal conductivity of the grouting material results in high $R_{\rm b}$ values. The exact in-situ position of the individual U-shaped pipes results in a major uncertainty which can hardly be quantified, even if a pipe spacer is used during installation.

The shank spacing will also be one of three factors in the focus of the present study. A number of studies are dedicated to factors determining the value of $R_{\rm b}$. Some studies examined the thermal borehole resistance of a single U-pipe BHE [16,19,20] and others focused on double U-pipe BHE [21,22]. However, these studies did not consider the evaluation of $R_{\rm b}$ using TRTs. Here, the effects of various pipe positions on the $R_{\rm b}$ values obtained from TRT interpretation will be analyzed and compared to actual ("true") $R_{\rm b-num}$ values determined by numerical simulation. In addition, the influence of the shank spacing on the resulting $\lambda_{\rm eff}$ will be evaluated. For this, valid pairs of estimated $R_{\rm b}$ and $\lambda_{\rm eff}$ values will be studied as a function of the shank spacing.

Signorelli et al. [13] demonstrated for one numerically simulated TRT that the non-uniform initial ground temperature distribution due to the natural vertical geothermal gradient, which is not considered by the line source theory, results in a detectable difference between the obtained $\lambda_{\rm eff}$ and the true thermal conductivity of the porous medium, $\lambda_{\rm m}$. Raymond et al. [12] confirm these findings by analyzing a TRT conducted in a waste rock. This

waste rock contains iron-sulfide minerals which react exothermally with water and oxygen and cause an abnormally high geothermal gradient (0.3 °C m $^{-1}$). The TRT is evaluated with a numerical model and based on the standard line source approach. The thermal conductivity value of the numerical analysis is approximately 14% lower than the value of the line source based evaluation. The work reported here was based on their findings and will focus on a systematic analysis of the influence of various non-uniform initial temperature distributions on the TRT result. Additionally, the correlation between $R_{\rm b}$ and $\lambda_{\rm eff}$ will be studied.

Several studies [13,6,14] evaluated the influence of convective heat transfer, i.e. groundwater flow, on TRT interpretation (in particular on λ_{eff}). However, these studies did not consider the effects of thermal dispersion. Although Raymond et al. [12] mentioned the need to also account for thermal dispersion in TRT interpretation, no sensitivity study was performed. In contrast to this, Molina-Giraldo et al. [23] found that dispersion-dominated aquifers result in smaller temperature changes close to the BHE and shorter thermal plumes (delineated by given temperature difference to the ambient aquifer). The present study will therefore also concentrate on the effects of thermal dispersion on the TRT and a detailed analysis of convection-influenced TRTs will be performed.

The main objective of this study is to obtain deeper insight into the influence of the three factors of shank spacing, non-uniform initial temperature distribution (e. g. geothermal gradient), and thermal dispersion on the interpretation of TRTs. Furthermore, the difference between estimated and true parameter values characterizing the BHE and subsurface under various conditions will be determined. For this purpose, a high-resolution finite element BHE model with coupled heat and mass transport will be developed to generate artificial TRT data sets with well-known initial and boundary conditions. The generated data will be analyzed by two common line source based evaluation approaches, linear regression and the two-variable parameter fitting method.

2. Methodology

2.1. Line source theory

Kelvin's line source theory [24] is often used to evaluate a TRT [4,5,13]. The BHE is approximated as an infinite line source in a homogeneous, isotropic, and infinite medium, which injects or

extracts a constant amount of energy (q). The temporal and spatial temperature changes around the line source are derived by [6,25]:

$$T_{\text{sub}}(r,t) - T_0 = \frac{q}{4\pi\lambda_{\text{eff}}} \int_{\frac{r^2}{4\kappa t}}^{\infty} \frac{e^{-u}}{u} du$$

$$= \frac{q}{4\pi\lambda_{\text{eff}}} \text{Ei} \left[\frac{r^2}{4\kappa t} \right] \approx \frac{q}{4\pi\lambda_{\text{eff}}} \left[\ln\left(\frac{4\kappa t}{r^2}\right) - \gamma \right]$$
(1)

where q [W m⁻¹] is the heat injection rate per unit length of a borehole, $\lambda_{\rm eff}$ [W m⁻¹ K⁻¹] the effective thermal conductivity of the subsurface, and κ [m² s⁻¹] the thermal diffusivity of the subsurface. The mean fluid temperature ($T_f = (T_{\rm in} + T_{\rm out})/2$ [13]) of the circulating heat carrier fluid can be accessed by including a thermal borehole resistance term, $R_{\rm b}$, in Eq. (1) [13]:

$$T_f - T_{\text{bw}} = qR_b \tag{2}$$

The thermal borehole resistance depends mainly on the geometry (shank spacing, pipe and well diameter, number of pipes, and depth of the BHE) as well as on the physical parameters of the BHE, such as thermal properties of the BHE material, flow rate of heat carrier fluid in the BHE, and fluid properties [26]. This yields:

$$T_{f}(t) = T_{\text{bw}}(t) + qR_{\text{b}} = \frac{q}{4\pi\lambda_{\text{eff}}} Ei \left[\frac{r_{\text{bw}}^{2}}{4\kappa t} \right] + T_{0} + R_{\text{b}}q \approx \frac{q}{4\pi\lambda_{\text{eff}}} \ln(t)$$

$$+ q \left[R_{\text{b}} + \frac{1}{4\pi\lambda_{\text{eff}}} \left(\ln\left(\frac{4\kappa t}{r_{\text{bw}}^{2}}\right) - \gamma \right) \right] + T_{0}$$
(3)

The logarithmic approximation of Eq. (3) is a linear function of the logarithm of time. One possibility to graphically evaluate the TRT is by linear regression of the measured fluid temperature in logarithmic time. The slope (m) of the straight line is used to quantify $\lambda_{\rm eff}$ as follows:

$$\lambda_{\text{eff}} = \frac{q}{4\pi m} = \frac{q}{4\pi} \frac{\ln(t_2) - \ln(t_1)}{T_f(t_2) - T_f(t_1)} \tag{4}$$

In the same manner, R_b is determined by the *y*-axis intercept. The other possibility consists in a more rigorous two-variable parameter fitting method [9]. This approach minimizes the misfit (e.g. root mean squared error, RMSE) between model and observation by a combined adjustment of R_b and λ_{eff} [18]:

RMSE =
$$\left[\frac{1}{n}\sum_{i=1}^{n} \left(T_{\text{mea}} - T_{f}\right)^{2}\right]^{0.5}$$
 (5)

Due to measurement impreciseness and data noise, no perfect fit can be obtained and instead of one optimal parameter combination, it is desirable to also evaluate valid parameter pairs of $R_{\rm b}$ and $\lambda_{\rm eff}$. Validity has to be decided on for each specific case and is determined by setting a threshold of tolerable RMSE. Here, the valid parameter pairs are searched for by exhaustive grid search. Reasonable intervals of $R_{\rm b}$ and $\lambda_{\rm eff}$ are discretized on a sufficient level of detail and interpolated response surfaces of fit are obtained through complete testing of all possible parameter pairs. In the current study the acceptable error of the parameter fitting method is set to an RMSE of 0.14 °C based on the typical uncertainty of the temperature difference of 0.14 °C determined by Witte et al. [5], which is supposed to represent the measurement error of a TRT.

2.2. Numerical simulation

In contrast to the application of the line source equation, numerical models allow for the simulation of coupled subsurface physical and hydraulic processes during a TRT. The numerical model can be used to simulate the relevant processes during a TRT under realistic conditions. Although using real field data would be even more desirable, synthetic simulations are attractive, since all processes and their specifications are completely known. By comparison to standard line source theory-based interpretation, the significance of the

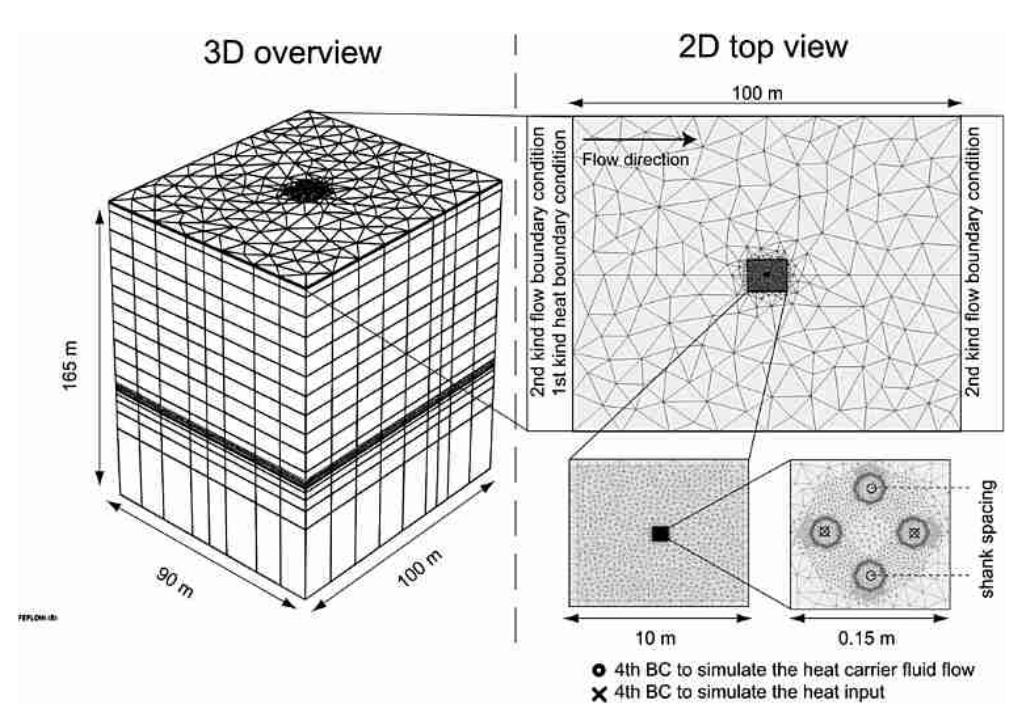


Fig. 1. Left: 3D overview of the model domain and discretization. Right: 2D top view of the model domain and the used boundary conditions (BC).

individual effects to the standard parameters, R_b and λ_{eff} , can be quantified accurately.

In previous studies, 1D finite difference BHE models [27], 2D finite volume BHE models [28], 2D finite element BHE models [17], 3D finite difference BHE models [15], and 3D finite element BHE models [13] were used. Due to the three-dimensionality of heat transport caused by a BHE in the subsurface, a 3D simulation is the most favourable option [13]. The complex geometry of a BHE can be represented by finite element meshes [29]. Therefore, finite element-based simulations are frequently used to simulate BHE [18,19,30,31]. A common and versatile commercial finite element software platform for computationally efficient simulations of 3D heat transport is FEFLOW [32].

Since the release of the FEFLOW version 5.4, a BHE model has been implemented directly in the software, in which the BHE is simulated as an embedded vertical 1D finite element in the finite element matrix [32]. However, this implementation does not provide the exact spatial temperature distribution inside the BHE. This prevents a detailed analysis of R_b based on numerical results. Within the framework of the present study, an alternative single BHE model based on the study by Signorelli et al. [13] was developed in FEFLOW and verified for conduction - as well as convection -dominated aguifer systems [33]. The BHE is assumed to be installed in a confined sandy aquifer. The flow field around a single BHE is hardly influenced by the BHE and therefore simulated in steady-state, whereas the heat transport is simulated transiently. The entire 3D model has a size of $100 \times 90 \times 165$ m (length \times width \times depth; Fig. 1), which is large enough to minimize boundary effects for the period of a TRT (e.g. 40-90 h). The dimensions of the fully discretized BHE are listed in Table 1.

The distance between borehole wall and the pipe wall is often unknown. To determine the uncertainty, several numerical simulations with varying pipe positions are analyzed. The model is discretized by 191,940 prism elements equally distributed in 35 horizontal layers. The finite element resolution is telescopic: It increases towards the BHE and reaches a maximum at the pipe wall (Fig. 1), where the steepest temperature gradients are expected. The distance between nodes varies between approximately 20 m at the model boundary and approximately 0.001 m at the pipe wall. The thickness of the horizontal layers ranges between 0.03 m and 39 m. The layer offset is smallest at the bottom of the BHE, where the highest vertical temperature gradients are expected.

Thermal and hydraulic properties of the different compartments of the finite element mesh are given in Table 2. The selected values are based on reported real values, except for the thermal conductivity of the pipe material and the part of the mesh representing the heat carrier fluid. The heat transfer between the turbulently flowing heat carrier fluid and the pipe wall can be approximated by a one-dimensional series connection of thermal resistances, which gives the fitted thermal conductivity of the pipe material. Due to turbulent flow within the BHE, lateral heat transfer to/from the heat carrier fluid is very fast. To represent this in the model, thermal conductivity of the elements representing the heat carrier fluid is set very high [31]. Clausen [34] demonstrated that a thermal conductivity of 20 W m⁻¹ K⁻¹ is sufficient to represent this turbulent flow. Furthermore, a modification of the volumetric heat

Table 1Detailed dimensions of the simulated borehole heat exchanger.

	Value
Radius of the borehole, r_b , (m)	0.075
Inner radius of the pipe, r_{pin} (m)	0.013
Outer radius of the pipe, r_{pout} (m)	0.016
Depth of the BHE, D_{BHE} (m)	100

Table 2 Hydraulic and thermal properties of different model compartments.

Property	Hydraulic conductivity, <i>K</i> , (m s ⁻¹)	Thermal conductivity of the porous media, λ_m , (W m ⁻¹ K ⁻¹)	Volumetric heat capacity of the porous media, cp , (MJ m $^{-3}$ K $^{-1}$)
Subsurface Grouting material Pipe material Heat carrier fluid	1.5×10^{-3a} [36] 6×10^{-8a} [38] 1×10^{-19c} [41] 1×10^{-19c} [41]	2.1 ^a [37] 0.8 ^a [38] 0.39 ^b [13] 20.0 ^b [34]	2.8^{a} [37] 2.3^{b} [39,40] 1.6^{a} [13] 1×10^{-6c} [35]
(mesh) Heat carrier fluid (discrete feature element)	-	0.6 ^a [13]	4.2 ^a [13]

- a Reported realistic values.
- ^b Estimated based on real values.
- ^c Estimated to be able to run the model and avoid hydraulic interactions between the discrete feature elements and the part of the FE mesh representing the grouting material and the subsurface

capacity for the part of the mesh representing the heat carrier fluid is recommended by Diersch et al. [35]. The volumetric heat capacity of this part should therefore be very small (e.g. 1 J m $^{-3}$ K $^{-1}$).

To simulate flow of the heat carrier fluid, elements of lower dimension, i.e. discrete feature elements [42], are often connected with the 3D finite element mesh [6,14,32]. The shank spacing of the simulated BHE is equal to the distance between the connected discrete feature elements representing the centre of each pipe (Fig. 1). Convective heat transport through the heat carrier fluid is simulated only within the discrete feature elements. Heat transport of the connected mesh representing the inner parts of the pipe is approximated by conduction only [32]. The flow of the heat carrier fluid is defined by a fourth-type boundary condition (BC) [32]. In FEFLOW the fourth-type BC describes a singular point source, which describes the injection or withdrawal rate of water/mass/ energy into/from a single node or into/from a number of nodes. To simulate the energy transfer to the circulating BHE fluid, a fourthtype BC is used. Constant values are assigned to both fourth-type BC, therefore the BHE fluid is circulating with a constant flow rate and a constant energy injection rate to BHE fluid. This arrangement is very similar to a TRT device used in the field. Here, the flow rate of the heat carrier fluid and the energy transfer to the heat carrier fluid are held constant by the TRT device. Thus, the heat transfer rate, q, of the simulated BHE can be calculated based on the

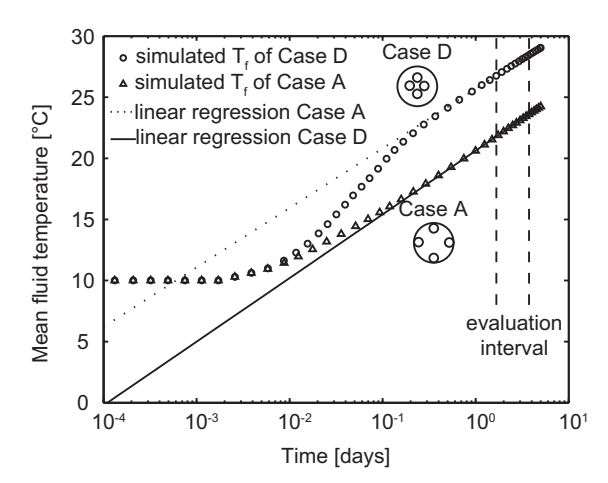


Fig. 2. Comparison of two numerically generated temperature time series of the mean fluid temperature T_f at variable shank spacings. Additionally, the result of the linear regression is presented.

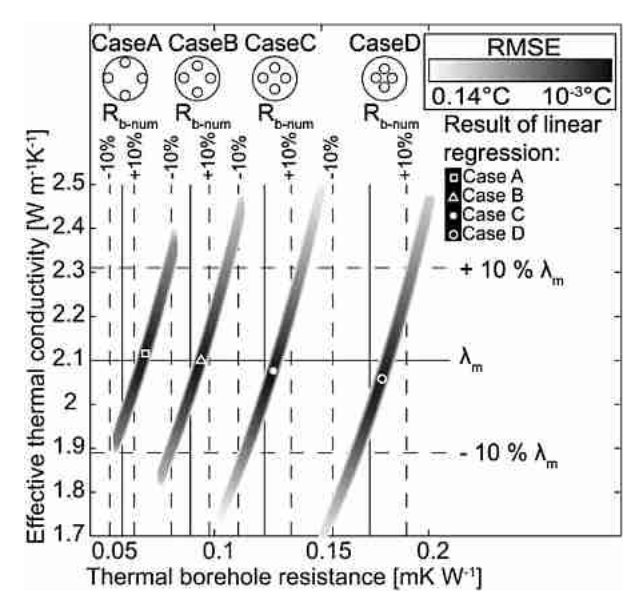


Fig. 3. Results of the two-variable parameter fitting method and the linear regression method for four different BHE shank spacings compared to the thermal conductivity of the porous media $(\lambda_{\rm m})$ and the $R_{\rm b-num}$ value. The evaluated time interval lasts from 40 h to 90 h and only parameter pairs with an RMSE value smaller than 0.14 °C are presented.

difference between inlet temperature, $T_{\rm in}$, and outlet temperature, $T_{\rm out}$, the volume flow rate of the heat carrier fluid, $Q_{\rm f}$, and the volumetric heat capacity of the heat carrier fluid, $c_{\rm pf}$.

$$q = \frac{cp_f Q_f (T_{\rm in} - T_{\rm out})}{L} \tag{6}$$

Based on Eq. (6) we calculated for each test case the average heat transfer rate, q, of the examined evaluation period of the BHE.

Groundwater flow, if applicable, is simulated by a second-type BC (Neumann) that assigns a constant flux to model boundary nodes [32]. The temperature of the groundwater, which enters the model domain, is controlled by a first-type BC (Dirichlet), which assigns a certain temperature value to a selected node [32].

The numerical model is applied to simulate a BHE, which injects energy of a known rate into the subsurface. The resulting synthetic time series of the temperature development of the heat carrier fluid represent the measured (artificial) data set of a TRT. In separate subsequent analyses, the influence of the geometry of the BHE as well as of naturally occurring non-uniform initial temperature distributions, e.g. vertical geothermal gradients and thermal dispersivities, on standard TRT-based interpretation are investigated. For this purpose, evaluation intervals of 50 h and a starting point of 40 h are selected, which is considered a period sufficient to obtain

reliable results [13]. Furthermore, to improve the comparability of the parameters obtained, equal starting points and the same duration of the evaluation interval are set for all experiments.

3. Results and discussion

By way of example, Fig. 2 illustrates two numerically generated TRT data sets. Additionally, the linear regression based on Eq. (3) is shown.

3.1. Pipe position

To exclusively analyze the effects of different shank spacings, no groundwater flow is considered and the initial temperature of the entire model is assumed to be uniform. These conditions comply with those commonly assumed for application of the line source equation. Different shank spacings are simulated by variants of the numerical model grid that is adjusted to the cross section geometry of the BHE. The setup of the models is illustrated in Fig. 3 showing different sections through the BHE, with decreasing distance of the symmetrically arranged tubes from Case A to D. The simulated shank spacings are 0.115 m, 0.092 m, 0.071 m, and 0.051 m in Cases A to D, respectively.

The results of the analysis are also presented in Fig. 3. For both parameter estimation techniques, the linear regression and the parameter fitting method, the effective thermal conductivities (λ_{eff}) identified sufficiently approximate the given thermal conductivity of the porous media (λ_m) . According to the way the parameter values are derived, they are further distinguished by $\lambda_{eff-lin}$ and $\lambda_{eff-lin}$ _{par}. Table 3 shows that the best fitted values of λ_{eff} are identical for both methods. Fig. 3 also reveals that several parameter pairs of λ_{eff} $_{\rm par}$ and $R_{\rm b-par}$ exist within the valid RMSE range (<0.14 °C). Valid pairs are positively correlated, indicating an ill-posed parameter estimation problem. If the acceptable error interval of estimated parameter values is set to $\pm 10\%$ [43], the detected pairs are mostly within these limits. With the given RMSE threshold, however, valid solutions spread beyond the 10% interval. Since the RMSE threshold is an arbitrary tolerance level that accounts for measurement uncertainty and noise, setting a stricter threshold may be problematic in practice, although this would improve identifiability of λ_{eff} and R_b in the ideal case.

The effective thermal conductivities obtained decrease with decreasing shank spacing and only in Case B is $\lambda_{\rm eff}$ similar to the "true" $\lambda_{\rm m}$ specified in the numerical model. Nevertheless, the differences between the $\lambda_{\rm eff-lin}$ and $\lambda_{\rm m}$ values obtained are small and lie within an interval of -2% and +1%. This demonstrates that the derived $\lambda_{\rm eff}$ is an apparent and integral value integrating the properties of the grouting material and the aquifer. In general, the smaller the shank spacing is and the larger the distance to the ambient ground, the greater is the influence of the grouting material and, hence, the smaller is the derived effective thermal

Table 3Results of linear regression and parameter fitting in comparison to originally simulated values ($\lambda_{\rm m}$ and $R_{\rm b-num}$) for four different shank spacings. The evaluated time interval is between 40 h and 90 h.

Pipe position	Case A	Case B	Case C	Case D
Shank spacing (m)	0.115	0.092	0.071	0.051
Heat transfer rate per unit length, calculated by Eq. (6), q (W m ⁻¹)	59	61	58	52
Thermal borehole resistance of the numerical simulation, $R_{b-\text{num}}$ (m K W ⁻¹)	0.057	0.089	0.124	0.173
Thermal borehole resistance determined by linear regression, $R_{\text{b-lin}}$ (m K W ⁻¹)	0.068	0.094	0.128	0.178
Thermal borehole resistance determined by parameter estimation, R_{b-par} m K W ⁻¹)	0.068	0.094	0.128	0.178
Thermal conductivity of porous media, λ_m (W m ⁻¹ K ⁻¹)	2.10	2.10	2.10	2.10
Effective thermal conductivity determined by linear regression, $\lambda_{\text{eff-lin}}$ (W m ⁻¹ K ⁻¹)	2.12	2.10	2.08	2.06
Effective thermal conductivity determined by parameter estimation, $\lambda_{\text{eff-par}}$ (W m ⁻¹ K ⁻¹)	2.12	2.10	2.08	2.06

conductivity. The overestimation by 1% determined for Case A is due the deviation of the simulated system from the ideal shape assumed by the line source. In this particular case, interpretation by a cylinder source equation appears to be more suitable.

In contrast to its minor influence on the interpretation of thermal conductivity, the effect of changing shank spacing on the best fitted value of R_b is significant (Fig. 3). This agrees with the observations by Acuna et al. [16], who studied the thermal borehole resistance of single U-pipe BHEs by a steady-state approach. We determined the same promoting effect of increasing shank spacing on R_b obtained by TRTs for a double U-pipe system. Again, the best results of the linear regression (R_{b-lin}) and the parameter fitting method (R_{b-par}) are in agreement. Borehole resistance values, R_{b-lin} and R_{b-par} , are comparable to those derived directly by Eq. (2) from the numerical model (R_{b-num}). For using this equation, the actual difference between borehole wall temperature (T_{bw}) and carrier fluid temperature (T_f) is determined by the simulated temperatures. T_f is extracted at the discrete feature element and T_{bw} is determined at eight equally scattered points on the borehole wall. To account for 3D effects, the weighted mean R_{b-num} value of four different layers (depth of 0 m, 15 m, 55 m, and 95 m) is calculated. The R_{b-num} value is considered to be most suitable for representing the actual heat transfer inside the BHE (Fig. 3).

The estimated values of R_{b-lin} and R_{b-par} agree with R_{b-num} within an interval of $\pm 10\%$, except for Case A. The reason of the higher discrepancy in this case is the direct contact between the pipes and the ambient ground, which substantially disturbs the temperature distribution at the borehole wall. Thus, the assumption of a uniform $T_{\rm bw}$ is not fulfilled and the standard $R_{\rm b}$ calculation method is no longer suitable. Due to the unrealistic shape of Case A, the evaluation procedure is not adopted for this test case. However, Case A is included in this study as it offers insight into the theoretically minimum possible value of R_b . Although the fitting error is small for the Cases C-D, the values of R_{b-lin} and R_{b-par} systematically overestimate R_{b-num} . This is interpreted as an indication of 3D effects explicitly simulated by the numerical model, but not covered by the line source equation. Case B represents intermediate conditions, where these artifacts appear to be negligible and the actual parameters $\lambda_{\rm m}$ and $R_{\rm b-num}$ can be estimated perfectly. Therefore, the remainder of this study will focus on the shank spacing simulated by Case B.

3.2. Non-uniform initial temperature distribution

To analyze the effects of a non-uniform initial temperature distribution of the subsurface on the TRT result, the model with the fixed pipe configuration of Case B is modified. While constant thermal and hydraulic material properties are kept as before (see Table 2) and groundwater flow is neglected, initial temperature increases with depth according to a specific geothermal gradient.

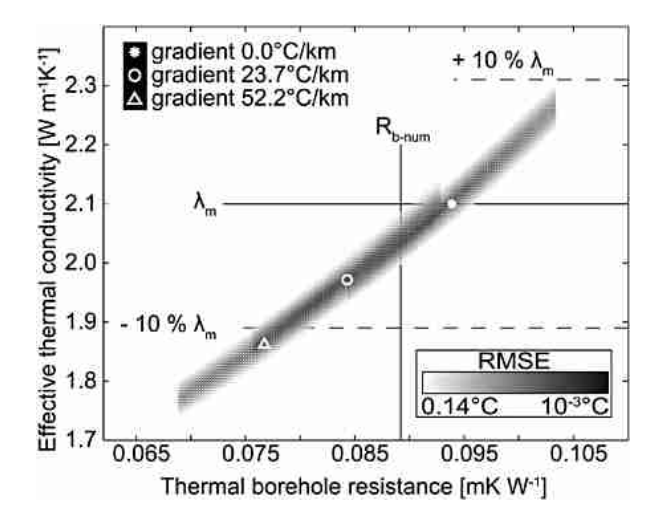


Fig. 4. Results of the two-variable parameter fitting method and the linear regression method for three different initial temperature distributions compared to the thermal conductivity of the porous media and the $R_{\rm b-num}$ values. The latter are given in Table 4. The evaluated time interval lasts from 40 h to 90 h and only parameter pairs with an RMSE value smaller than 0.14 °C are presented here.

To simulate realistic geothermal gradients, the initial temperature field is calculated separately by steady-state simulations with different geothermal heat fluxes at the bottom boundary of the model and a constant temperature at the surface of the model (Table 4).

According to Pollack et al. [44], a geothermal heat flux range between 0.05 and 0.11 W m $^{-2}$ is considered to be realistic. Based on the given extreme values, temperature gradients of 23.7 °C km $^{-1}$ and 52.2 °C km $^{-1}$ are determined for the numerical model, which are below the unnaturally high gradient of 300 °C km $^{-1}$ analyzed in the special case by Raymond et al. [12]. The initial ambient temperature values in the model are calculated based on the two temperature gradients selected and assuming a fixed temperature value of 10 °C at a depth of 50 m. In this way, the simulations of the two geothermal gradients remain comparable.

Both line source evaluation approaches yield comparable results (relative difference less than 1%). However, the best fitted λ_{eff} values are smaller than the input values of the numerical simulation selected (Fig. 4). For high geothermal gradients (52.2 °C km $^{-1}$), the acceptable error exceeds $\pm 10\%$ (Fig. 4) [43]. Fig. 4 illustrates again that a wide range of valid parameter pairs of $\lambda_{eff-par}$ and R_{b-par} exists and acceptable parameter values are correlated positively. This validity range is shifted along the direction of correlation by increasing the value of the geothermal gradient. This outcome demonstrates that a depth-dependent initial temperature field prevents reliable line source based TRT evaluation. The geothermal gradient influences the horizontal temperature gradient towards

Table 4Results of the parameter fitting method, linear regression, and the FEFLOW input values ($\lambda_{\rm m}$ and $R_{\rm b-num}$) for three different initial temperature distributions which can be described by a constant geothermal gradient. All simulations are based on a BHE with the geometry of Case B. The evaluated time interval is between 40 h and 90 h.

Heat flux (W m^{-2}):	0.00	0.05	0.11
Resulting geothermal gradient (${}^{\circ}$ C km $^{-1}$):	0.0	23.7	52.2
Heat transfer rate per unit length, calculated by Eq. (6), q (W m ⁻¹)	61	58	55
Thermal borehole resistance of the numerical simulation, $R_{b-\text{num}}$ (m K W ⁻¹)	0.089	0.089	0.089
Thermal borehole resistance determined by linear regression, $R_{\text{b-lin}}$ (m K W ⁻¹)	0.094	0.084	0.077
Thermal borehole resistance determined by parameter estimation, R_{b-par} (m K W ⁻¹)	0.094	0.083	0.077
Thermal conductivity of porous media, $\lambda_{\rm m}$ (W m $^{-1}$ K $^{-1}$)	2.10	2.10	2.10
Effective thermal conductivity determined by linear regression, $\lambda_{\text{eff-lin}}$ (W m ⁻¹ K ⁻¹)	2.10	1.97	1.86
Effective thermal conductivity determined by parameter estimation, $\lambda_{eff-par}$ (W m ⁻¹ K ⁻¹)	2.10	1.96	1.86

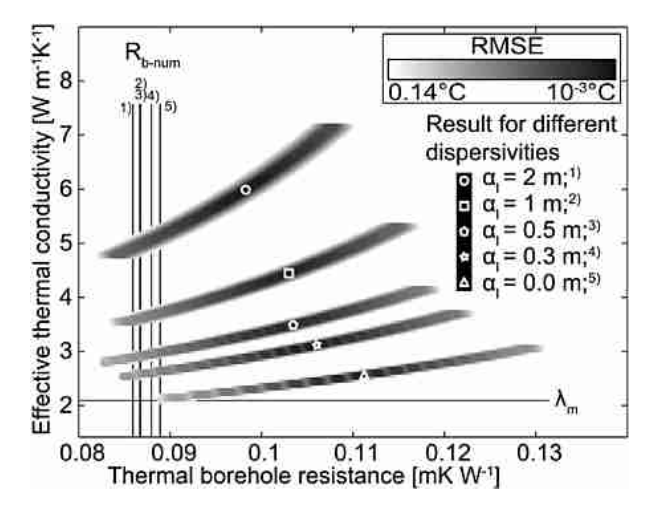


Fig. 5. Result of the two-variable parameter fitting method and the linear regression method for five different thermal dispersivities (constant Darcy velocity of 0.1 m day $^{-1}$) compared to the thermal conductivity of the aquifer and the $R_{\rm b-num}$ values. The latter are given in Table 5. The evaluated time interval lasts from 40 h to 90 h and only parameter pairs with an RMSE value smaller than 0.14 $^{\circ}$ C are presented. Superscript numbers specify the thermal dispersivities belonging to a corresponding $R_{\rm b-num}$ value.

the BHE. The amplified depth-dependent heat propagation which cannot be considered by the line source theory leads to an apparently higher thermal conductivity than the real one.

As shown above, the borehole resistance $R_{\rm b}$ reflects the heat transport inside the BHE and, thus, depends on geometry and physical properties of the BHE itself. Hence, it can be expected that R_b is quasi-independent of the subsurface properties and that the TRT parameter values obtained are constant and comparable to those computed for the negligible geothermal gradient (0.089 m K W⁻¹, Table 3). This is true for the value of $R_{\rm b-num}$ which is determined directly from the numerical model (Table 4). In contrast to this, $R_{\rm b-lin}$ and $R_{\rm b-par}$ values obtained from the TRT seem to be influenced significantly by the geothermal gradient (Table 4).

For the geothermal gradients evaluated, the resulting $R_{b-\text{lin}}$ and $R_{b-\text{par}}$ values vary in the range between 0.077 m K W⁻¹ and 0.094 m K W⁻¹. The line source based TRT evaluation with a constant initial temperature yields the slightly overestimated value of $R_b = 0.094$ m K W⁻¹ (see Fig. 3). At an enhanced geothermal gradient, the estimated value of R_b decreases. The relative error of the line source evaluation for the high geothermal gradients selected even exceeds the acceptable error range of $\pm 10\%$ (Fig. 4) [43]. This relationship between estimated borehole resistance and geothermal gradient apparently is artificial and does not represent the real heat transfer inside the BHE. This positive correlation illustrated in Fig. 4 might be caused by the temperature variations inside and outside the BHE along the total length, leading to depth-dependent R_b values.

3.3. Thermal dispersion

A third aspect analyzed is the effect of longitudinal and transverse thermal dispersion on TRT interpretation. Again, artificial TRT data sets are generated using the numerical model that simulates a BHE with the pipe configuration of Case B. A uniform horizontal Darcy velocity of 0.1 m day $^{-1}$ is assumed for the aquifer. This threshold is recommended by Signorelli et al. [13] to be the upper limit for TRT evaluations based on the line source theory. The thermal dispersivities are varied and a constant relationship $\alpha_{\rm T}=0.1\times\alpha_{\rm L}$ is assumed [23]. Molina-Giraldo et al. [23] demonstrate the variability of the reported $\alpha_{\rm L}$ and $\alpha_{\rm T}$ values which are mainly influenced by the relationship applied for the description of thermal dispersion. Hence, a wide range of $\alpha_{\rm L}$ values between 0 and 2 m is analyzed here in order to represent possible values for a field scale of 10 m [23]. The results are depicted in Fig. 5.

Both parameter estimation techniques yield similar $\lambda_{eff-lin}$ and $\lambda_{eff-par}$ values with a difference of less than 1% (Table 5). Both evaluation approaches are therefore considered to be equally suitable for the TRT-based λ_{eff} determination in these cases. Again, the parameter estimation with an RMSE tolerance of 0.14 °C yields a correlated group of $\lambda_{\rm eff-par}$, $R_{\rm b-par}$ pairs. The $\lambda_{\rm eff}$ values obtained are significantly higher than the original value of λ_m in the numerical model. They are higher than λ_m by a factor between 20% ($\alpha_L=0$) and 190% ($\alpha_L=2$), which clearly exceeds the acceptable 10% error assumed for a TRT [43]. The effect of increasing thermal dispersivity on the valid λ_{eff} value range is explained by the relationship between $\alpha_{\rm L}$ and $\alpha_{\rm T}$ and the effective thermal dispersion coefficient which is one key parameter of the heat transport equation in porous media [45]. Heat transport, including dispersion, results in an increase of λ_{eff} (Table 5). Thus, TRT evaluation of convection-dominated conditions should not only consider the effect of convection, but also the impact of dispersion.

As in all previous results, the R_{b-lin} and R_{b-par} values obtained are identical. A slightly negative correlation between thermal dispersivity and determined borehole resistance is found. The calculated R_{b-num} values decrease by up to 3% compared to the conduction-dominated value of 0.089 m K W⁻¹ (Table 3). The decrease by 3% might be caused by dispersive effects into the BHE, which decrease the thermal resistance between the borehole wall and the heat carrier fluid. This is also reflected by the line source based best estimates of R_b . However, these values are significantly higher than those in the model. They also span a broad validity range depending on the given dispersivity. By neglecting the effects of thermal dispersion, the best line source based fit yields an overestimation of 14% compared to R_{b-num} . This discrepancy increases with the degree of dispersion up to 25% for $\alpha_L = 2$ m. Under these conditions, the standard line source equation obviously is not applicable. Consequently, estimated parameter values are not reliable.

Results of the two-variable parameter fitting method, the linear regression method, and the FEFLOW input values ($\lambda_{\rm m}$ and $R_{\rm b-num}$) for six different thermal dispersivity values. The evaluated time interval is 40–90 h.

Longitudinal dispersivity, α_L (m)	2	1	0.5	0.3	0
Heat transfer rate per unit length, calculated by Eq. (6), q (W m ⁻¹)	61	61	61	61	61
Thermal borehole resistance of the numerical simulation, $R_{\text{b-num}}$ (m K W ⁻¹) Thermal borehole resistance determined by linear regression, $R_{\text{b-lin}}$ (m K W ⁻¹) Thermal borehole resistance determined by parameter estimation, $R_{\text{b-par}}$ (m K W ⁻¹) Thermal conductivity of porous media, λ_{m} (W m ⁻¹ K ⁻¹) Effective thermal conductivity determined by linear regression, $\lambda_{\text{eff-lin}}$ (W m ⁻¹ K ⁻¹) Effective thermal conductivity determined by parameter estimation, $\lambda_{\text{eff-par}}$ (W m ⁻¹ K ⁻¹)	0.086	0.087	0.087	0.088	0.089
	0.098	0.103	0.103	0.106	0.111
	0.098	0.103	0.103	0.106	0.111
	2.10	2.10	2.10	2.10	2.10
	5.99	4.44	3.48	3.11	2.56
	6.00	4.45	3.49	3.13	2.58

4. Conclusions

A finite element model of a double U-pipe BHE was developed to generate artificial TRT data sets. Based on these data sets, the influence of selected natural subsurface conditions, such as depth-dependent temperature variation and thermal dispersion, was investigated. Furthermore, the effect of the shank spacing within the BHE on TRT interpretation was assessed by simultaneous $\lambda_{\rm eff}$ and $R_{\rm b}$ estimation. From the results of this study, the following conclusions can be drawn:

- The TRT parameters (R_{b-lin} , R_{b-par} and $\lambda_{eff-lin}$, $\lambda_{eff-par}$) obtained for different shank geometries represent the real parameters of the subsurface (λ_m) and the BHE (R_{b-num}) with sufficient accuracy. The shank spacing analyzed varied between 0.051 and 0.115 m, the resultant error of the estimated λ_{eff} values was less than 2%. However, the borehole resistance is strongly dependent on the shank spacing. With increasing shank spacing, the borehole resistance decreases as the influence of the grout material is reduced. At the same time, the error of line source based R_b estimation increases. The BHE more and more disagrees with the ideal line-shaped heat source. In practice, a TRT evaluation based on the cylinder source equation, which was analyzed by Sass and Lehr [46], might improve the result for large shank spacing, such as in Case A.
- A typical geothermal gradient (0 °C per 100 m to 5.2 °C per 100 m) results in an underestimation of λ_{eff} and R_b by the standard line source based approach. The estimation error may exceed 10% for a gradient of 5.2 °C per 100 m. This has to be accounted for when TRTs are conducted in areas with a relatively high geothermal gradient. Furthermore, the effects observed may also be induced by artificial temperature variations in the subsurface, for instance, by surrounding geothermal systems, local heat sources, such as sewage systems or other underground facilities, especially in urban areas.
- Apart from convection, also thermal dispersion was found to influence the TRT and its interpretation. Numerically generated TRTs influenced by a constant Darcy velocity (0.1 m day $^{-1}$) and various dispersivities (α_L between 0 and 2 m) result in a deviation from the "true" values of the model from 0.5 to 3.9 W m $^{-1}$ K $^{-1}$ for λ_{eff} and from 0.012 to 0.022 m K W $^{-1}$ for R_b , respectively. Hence, further studies of convection-dominated TRTs should also consider the effects of thermal dispersion. In practice, we recommend to consider not only groundwater flow, but also the effects of thermal dispersion for convection-influenced TRTs in highly heterogeneous aquifers.

This numerical study clearly showed the limits of the standard TRT evaluation when the test performed is influenced by extreme shank spacing, high geothermal gradients or significant dispersivity values. To overcome this restriction, improved concepts are needed to consider and quantify the analyzed effects, especially thermal dispersivity. TRT interpretation also has to account for feasible parameter ranges instead of best fits within a small function fitting tolerance only. The results of the numerical study here showed that typical case-specific valid ranges of positively correlated borehole resistance and effective thermal conductivity values exist.

Acknowledgements

We would like to thank Sofie Jehle, Nelson Molina-Giraldo, Joszef Hecht-Méndez, and one anonymous reviewer for their fruitful comments. Furthermore, the support of Maike Schröder in preparing the manuscript is also gratefully acknowledged.

References

- Blum P, Campillo G, Münch W, Kölbel T. CO₂ savings of ground source heat pump systems - a regional analysis. Renewable Energy 2010;35:122-7.
- [2] Saner D, Juraske R, Kübert M, Blum P, Hellweg S, Bayer P. Is it only CO₂ that matters? A life cycle perspective on shallow geothermal systems. Renewable and Sustainable Energy Reviews 2010;14:1798–813.
- [3] Morgensen P. Fluid to duct wall heat transfer in duct system heat storage. International conference on surface heat storage in theory and practice; 1983. Stockholm, Sweden.
- [4] Gehlin S. Thermal response test: in situ measurements of thermal properties in hard rock. Licentiate thesis. Sweden: Lulea University of Technology; 1998
- [5] Witte HJL, van Gelder GJ, Spitler JD. In-situ measurements of ground thermal conductivity: the Dutch perspective. ASHRAE Transactions: Research 2002; 108(1):263–72.
- [6] Witte HJL. Geothermal response test with heat Extraction and heat injection: examples of application in research and design of geothermal ground heat exchangers. Europäischer Workshop über Geothermische response tests; 2001. Lausanne. Switzerland.
- [7] Kübert M, Walker-Hertkorn S, Voutta A. Temperaturtiefenprofile stärken die Aussagekraft von thermal response tests. bbr-Fachmagazin für Brunnen und Leitungsbau oberflächennahe Geothermie 2009;60(9):38–43.
- [8] Esen H, Inalli M. In-situ thermal response test for ground source heat pump system in Elazig, Turkey. Energy and Buildings 2009;41:395–401.
- [9] Roth P, Georgiev A, Busso A, Barraza E. First in situ determination of ground and borehole thermal properties in Latin America. Renewable Energy 2004; 29(12). 1947–1963.
- [10] Sanner B, Hellström G, Spitler J, Gehlin S. Thermal response test current status and world wide application, World Geothermal Congress; 2005. Antalya, Turkey.
- [11] Gustafsson AM, Westerlund L. Multi-injection rate thermal response test in groundwater filled borehole heat exchanger. Renewable Energy 2010;35: 1061-70.
- [12] Raymond J, Therrien R, Gosselin L, Lefebvre R. Numerical analysis of thermal response tests with a groundwater flow and heat transfer model. Renewable Energy 2011;36(1):315–24.
- [13] Signorelli S, Bassetti S, Pahud D, Kohl T. Numerical evaluation of thermal response tests. Geothermics 2007;36(2):141–66.
- [14] Gehlin S, Hellstrom G. Influence on thermal response test by groundwater flow in vertical fractures in hard rock. Renewable Energy 2003;28(14):2221–38.
- [15] Wagner R, Clauser C. Evaluating thermal response tests using parameter estimation for thermal conductivity and thermal capacity. Journal of Geophysics and Engineering 2005;2(4):349–56.
- [16] Acuna J, Palm B. Local conduction heat transfer in U-pipe borehole heat exchangers. COMSOL Conference 2009. Milan, Italy.
- [17] Zanchini E, Terlizzese T. Finite-element evaluation of thermal response tests performed on U-tube borehole heat exchangers. COMSOL Conference 2008. Hanover, Germany.
- [18] Marcotte D, Pasquier P. On the estimation of thermal resistance in borehole thermal conductivity test. Renewable Energy 2008;33:2407–15.
- [19] Lamarche L, Kajl S, Beauchamp B. A review of methods to evaluate borehole thermal resistances in geothermal heat-pump systems. Geothermics 2010;39: 187–200.
- [20] Sharqawy MH, Mokheimer EM, Badr HM. Effective pipe-to-borehole thermal resistance for vertical ground heat exchangers. Geothermics 2009;38: 271-7.
- [21] Zeng H, Diao N, Fang Z. Heat transfer analysis of boreholes in vertical ground heat exchangers. International Journal of Heat and Mass Transfer 2003;46: 4467–81.
- [22] De Carli M, Tonon M, Zarrella A, Zecchin R. A computational capacity resistance model (CaRM) for vertical ground-coupled heat exchangers. Renewable Energy 2010:35:1537—50.
- [23] Molina-Giraldo N, Bayer P, Blum P. Evaluating the influence of thermal dispersion on temperature plumes from geothermal systems using analytical solutions. International Journal of Thermal Sciences 2011;50:1223–31.
- [24] Carslaw HS, Jaeger JC. Conduction of heat in solids. New York: Oxford University Press; 1959.
- [25] Gehlin S. Thermal response test method development and evaluation. Doctoral thesis. Sweden: Lulea University of Technology; 2002.
- [26] Pahud D, Matthey B. Comparison of the thermal performance of double U-pipe borehole heat exchangers measured in situ. Energy and Buildings 2001;33:503-7.
- [27] Shonder JA, Beck JV. Determining effective soil formation thermal properties from field data using a parameter estimation technique. ASHRAE Transactions: Symposia 1999;105(1):458–66.
- [28] Yavuzturk C, Spitler JD, Rees SJ. A transient two-dimensional finite volume model for the simulation of vertical U-tube ground heat exchangers. ASHRAE Transactions 1999;105(2):465–74.
- [29] Esen H, Inalli M, Esen Y. Temperature distributions in boreholes of a vertical ground-coupled heat pump system. Renewable Energy 2009;34:2672–9.
- [30] Diersch HJG, Bauer D, Heidemann W, Rühaak W, Schätzl P. Finite element modeling of borehole heat exchanger systems part 1. Fundamentals. Computer and Geosciences; 2010. doi:10.1016/j.cageo.2010.08.003.

- [31] Diersch HJG, Bauer D, Heidemann W, Rühaak W, Schätzl P. Finite element modeling of borehole heat exchanger systems part 2. Numerical simulation. Computer and Geosciences; 2010. doi:10.1016/j.cageo.2010.08.002.
- [32] Diersch HJG, FEFLOW 5.3 User's manual, Berlin: WASY GmbH; 2006.
- [33] Wagner V. Analysis of thermal response tests using advanced analytical and high resolution numerical simulations. Diploma thesis. Germany: Eberhard-Karls Universität Tuebingen; 2010.
- [34] Clausen H. Durchführung von Simulationsrechnungen zum Einfluss verschiedener Randbedingungen auf die thermische Leistungsfähigkeit von Erdwärmesonden, Diploma thesis. Germany: University Stuttgart; 2008.
- [35] Diersch HJG, Bauer D, Heidemann W, Rühaak W, Schätzl P. Finite element formulation for borehole heat exchangers in modeling geothermal heating systems by FEFLOW. WASY Software FEFLOW White Paper 2010;5:5–96.
- [36] Hähnlein S, Molina-Giraldo N, Blum P, Bayer P, Grathwohl P. Ausbreitung von Kältefahnen im Grundwasser bei Erdwarmesonden. Grundwasser 2010;15: 123–33.
- [37] Palmer CD, Blowes DW, Frind EO, Molson JW. Thermal energy storage in an unconfined aquifer 1. Field injection experiment. Water Resources Research 1992:28:2845–56
- [38] Hermann J. Ingenieurgeologische Untersuchungen zur Hinterfüllung von Geothermie-Bohrungen mit Erdwärmesonden. Doctoral thesis. Germany: Fridericiana University of Karlsruhe; 2008.

- [39] Niekamp A, Unklesbay K, Unklesbay N, Ellersieck M. Thermal properties of bentonite-water dispersions used for modeling foods. Journal of Food Science 1984;49:28–31.
- [40] Gauthier C, Lacroix M, Bernier H. Numerical simulation of soil heat exchangerstorage systems for greenhouses. Solar Energy 1997;60:333–46.
- [41] Pannike S, Kölling M, Panteleit B, Reichling J, Scheps V, Schulz HD. Auswirkung hydrogeologischer Kenngrößen auf die Kältefahnen von Erdwärmesondenanlagen in Lockersedimenten. Grundwasser 2006;11: 6–18
- [42] Diersch HJG. Discrete feature modeling of flow, mass and heat transport processes by using FEFLOW. WASY Software FEFLOW White Paper 2005;1: 151–98.
- [43] Eugster WJ. Angewandte Forschung: Workshop zur Qualitätssicherung von geothermischen response tests. Final report. Bern, Switzerland: Swiss Federal Office of Energy; 2002.
- [44] Pollack HN, Hurter SJ, Johnson JR. Heat flow from the earth's interior: analysis of the global data set. Reviews Ofgeophysics 1993;31:267—80.
- [45] Domenico PA, Schwartz FW. Physical and chemical hydrogeology. New York: John Wiley & Sons Inc; 1998.
- [46] Sass I, Lehr C. Improvements on the thermal response test evaluation applying the cylinder source theory. Thirty-sixth Workshop on Geothermal Reservoir engineering 2011. Stanford, United States of America.